# Buckling instabilities of a confined colloid crystal layer

T. Chou and David R. Nelson
*Department of Physics, Harvard University, Cambridge, Massachusetts 02138*
(Received 18 June 1993)

A model predicting the structure of repulsive, spherically symmetric, monodisperse particles confined between two walls is presented. When plate separations are small, only one layer of particles can be confined; however, when the plate separation is increased, multiple layers will eventually form. We study the buckling transition of a single flat layer as the double-layer state develops. Experimental realizations of this model are suspensions of stabilized colloidal particles squeezed between glass plates. By expanding the thermodynamic potential about a flat state of $N$ confined colloidal particles, we derive a free energy as a functional of in-plane and out-of-plane displacements. As the gap separation increases, certain out-of-plane modes soften. The wave vectors of these first buckling instabilities correspond to three different ordered structures. Landau theory predicts that the symmetry of these phases allows for second-order phase transitions. This possibility exists even in the presence of gravity or plate asymmetry. These transitions lead to critical behavior and phases with the symmetry of the three-state and four-state Potts models, the $X$-$Y$ model with sixfold anisotropy, and the Heisenberg model with cubic interactions. The experimental detection of these structures is discussed.

PACS number(s): 82.70.Dd, 46.30.Lx, 63.75.+z

## I. INTRODUCTION

Colloid suspensions have long been used in practical applications such as paints, coatings, and many manufacturing processes [1]. Recently, new uses of colloids such as in electro-optic devices and in semiconductors have been discovered [2]. These new uses, as well as the general understanding of colloidal ordering applicable in other fields, require a thorough knowledge of the structures and phases present in these suspensions. Hence, colloid structure and rheology have been under intense study across many disciplines [2].

Colloid particles, usually on the order of $1\mu$m in diameter, are a convenient size for laboratory study. Due to the complicated interactions these particles experience, colloid suspensions exhibit a rich cornucopia of phases in solution. These interactions can be described by electrostatic, van der Waals, hydrodynamic, and steric effects. When repelling moieties such as polymers or charged molecules are attached to the surfaces, the colloids are stabilized against aggregation and extended ordered structures in solution can form. Debye-Huckel theory is typically used to model the screened electrostatic interactions in a charge stabilized suspension. Electrostatic effects, together with van der Waals and hard sphere interactions, are important ingredients in the Derjaguin-Landau-Verwey-Overbeek (DVLO) theories [1].

In bulk, monodisperse colloidal systems can appear in liquid, crystalline, amorphous, and inhomogeneous phases. Crystals with bcc, fcc, and random stacked close packed structures have been observed [3].

Theoretically, the ordering of hard or otherwise repulsive spheres has been approached analytically and via computer simulations. Much effort has been directed towards understanding the nature and consequences of DVLO pair potentials. A Yukawa interaction was found to give rise to structural features consistent with observations [4]. Pair potentials have also been used to described the dynamics of colloid crystals [5].

Experimentally, these systems have been studied with microscopy, video imaging, and light diffraction [6–8]. In bulk, monodisperse colloidal systems can appear as liquid, crystalline, amorphous, and inhomogeneous states. Crystals with bcc, fcc, and random stacked close packed structures have been observed [1,3,9].

It was quickly realized that colloid suspensions are an ideal system to use for studying two-dimensional phase transitions. The first observation of 2D ordering was the interfacial colloidal crystal of Pieranski [10]. In this system, colloid particles floating on an air-water interface interact mainly through dipole-dipole forces. Subsequent studies have involved immersed colloids with regions where two plates are brought close together. The plates are immersed in bulk solution allowing for free expansion of the confined structures. In addition, by using materials such as poly(styrene), which is almost density matched to the aqueous solvent, the effects of gravity are negligible. In these studies, the bulk solution provides a fixed chemical potential and thermodynamic particle reservoir for the confined sample.

One class of experiments for which confined colloidal systems are particularly suited is the study of melting in two dimensions [6]. Because of their macroscopic size, colloid spheres do not feel the atomic scale granularity of the confinement walls (see Fig. 1). Thus, this system is an ideal candidate for observing dislocation and disclination driven melting mechanisms in 2D. In fact, the search for defect mediated melting appears to be most successful in these confined colloidal systems. An isotropic fluid exists at narrow wall separations; as $h$ is increased, the one-layer areal density increases. In practice, $h$ is dif-

 

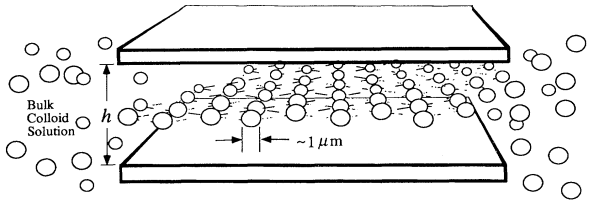


FIG. 1. A confined layer of repelling colloid particles.

ficult to accurately control and a wedge geometry with gradually increasing plate separation is used. The correlations of particle positions along this wedge are consistent with a two-stage dislocation-disclination mediated melting process.

If $h$ is increased further, the continual invasion of particles into the gap is allowed only by formation of multiple layers. The observations of many experimenters [6,7] can be summarized by

$$0 \to \text{fluid} \to 1\triangle \to 2\square \to 2\triangle \to \cdots \to N\square \to N\triangle \to (N+1)\square, \quad (1.1)$$

where the gap $h$ increases from left to right and $\triangle$ and $\square$ represent triangular and square lattices within each of the $N$ layers. In the gap, packing constraints dictate whether the layers are square or triangularly ordered [11]. The $\square$ and $\triangle$ layers are approximately the (001) and (111) planes of bcc and fcc lattices, respectively. As these transitions proceed, Murray and co-workers [6] have observed that large fluctuations of the colloids perpendicular to the plane occur; such fluctuations are especially prevalent in the $1\triangle \to 2\square$ transition. As $N$ increases, the structure of the confined layers approaches that of a bulk solution. In this study, we use static colloidal particle interactions to model the free energy of the assembly as a function of particle displacements. Stability conditions are imposed and minimization based on the Landau theory of structural phase transitions [12,13] is used to predict the possible buckled structures in the $1\triangle \to 2\square$ region. The free energy depends upon both the amplitude and phase of these "buckling waves."

In the next section, we derive from microscopic interactions the free energy of the confined colloid system. Stability of this model and the critical wave vectors are examined in Sec. III. The phase transition into each of the possible states is related to continuum statistical models in Sec. IV. Structure factors and other experimental consequences of these structures are then briefly discussed in Sec. V. Finally, a model for particles trapped in a tubular pore is presented in the Appendix.

## II. MODEL FREE ENERGY

In this section, we derive a free-energy functional from the thermodynamic potential of a confined layer of particles immersed in a bulk particle reservoir, neglecting many-body and hydrodynamic interactions which may be important [3]. The functional is written in terms of particle displacements and cast into the Landau-Ginzburg form. The parameters in this expansion are defined by the microscopic interactions in the problem.

For a confined collection of $N$ particles mutually interacting via a spherically symmetric potential $U(r)$, the free energy can be written as a sum over particles $i$ and $j$,

$$\Omega = \sum_{\substack{i,j \\ i<j}} U(|\vec{r}_i - \vec{r}_j|) + V(f_i, h) - \mu N, \quad (2.1)$$

where

$$V(f,h) = V_1\left(\frac{h}{2} - f\right) + V_2\left(\frac{h}{2} + f\right) + V_{\text{ext}}(f) \quad (2.2)$$

is the total particle-plate potential. $V_1$ and $V_2$ are the individual plate-layer potentials, which we usually assume equivalent when the confining plates are identical. The term $V_{\text{ext}}(f)$ describes the effects of external fields such as gravity. In that case $V_{\text{ext}} \propto f$. The $\hat{\mathbf{z}}$ component of $\vec{r}_i$ is denoted by $f_i$, the height of particle $i$ measured from the minimum of $V_1 + V_2$.

For a single layer of spheres squeezed between the plates just prior to buckling, the mean particle positions form a flat triangular lattice with lattice constant $a$. Although in two dimensions there is only quasi-long-range translational order [14], we will consider a finite sample that is locally crystalline. Assuming our $N$-particle sample is within a well ordered domain, the sum over all nearest-neighbor interactions becomes

$$\frac{\Omega_0}{A_0} = \frac{3NU(a_1) + 3NU(a_2) + \cdots - \mu N + V(0,h)N}{N(a^2\sqrt{3}/2)}, \quad (2.3)$$

where $A_0 = Na^2\sqrt{3}/2$ is the area occupied by the undistorted $N$-particle lattice. The last term varies with position in the wedge geometry of [6]: this experimental arrangement is equivalent to slow spatial variation in the chemical potential. The second and further terms on the right result from summing interparticle energies from next- and further-neighbor particles, respectively; hence, $a_1 \equiv a, a_2 = a\sqrt{3}$, etc.

For (2.3) to be useful, the further-neighbor interactions must be truncated at a suitable distance much smaller than the $N$-particle system size. Upon minimizing $\Omega_0/A_0$ with respect to $a$, we find the equilibrium lattice spacing and the chemical potential associated with it.

The lattice spacing $a$ depends on the strengths of the particle interactions and the chemical potential. However, the screening length of the interparticle potential is a function of ionic strength, which, due to charge neutrality, depends on the colloidal particle density. Therefore, the particle interactions indirectly depend on the chemical potential. We only use the $N\mu$ term as a device to illustrate how a regular lattice of colloid particles can exist. The spacing is still uniquely determined if the effective $U(r)$ is smooth and has at most one minimun. However, further-neighbor interactions and interactions with mul-

tiple minima could lead to phase transitions among flat structures of varying lattice constants $a$. Multiple minima are often predicted by the various contributions to interparticle potentials. We will assume that the repulsive part of the potential is strong enough to prevent aggregation and that there are no in-plane lattice distortions near the buckling transition when $f$ becomes nonzero. The necessary requirements on $U(r)$ will be determined below.

Upon expanding the total free energy about the flat phase $f = 0$ and about an equilibrium spacing $a = |\mathbf{x}_i - \mathbf{x}_j|$ between nearest neighbors $i, j$, with the definition of the in-plane displacement field $\mathbf{u}(\mathbf{x}_{j+i}) - \mathbf{u}(\mathbf{x}_j) + \mathbf{a}_i^n = \mathbf{x}_i - \mathbf{x}_j$, we have

$$\Omega = \sum_{\mathbf{x}} \sum_{n} \sum_{i=1}^{3} U\left(\sqrt{|\mathbf{u}(\mathbf{x}) - \mathbf{u}(\mathbf{x}+\mathbf{a}_i^n) - \mathbf{a}_i^n|^2 + |f(\mathbf{x}) - f(\mathbf{x}+\mathbf{a}_i^n)|^2}\right) + \sum_{x} V(f(\mathbf{x})) - \mu(a)N. \tag{2.4}$$

Here, $\sum_{\mathbf{x}}$ is a discrete sum over the sites of a triangular lattice and $n$ indexes different coordination shells. The $\{\mathbf{a}_i^n\}$ are the three vectors $\{i\}$ spanning the triangular lattice and inclined at 120° to each other, each with length $a_n$, as depicted in Fig. 2. For nearest neighbors,

$$\frac{1}{a_1}\{\mathbf{a}_i^1\} \equiv \{\mathbf{e}_i^1\} \equiv \left\{\hat{\mathbf{y}}, \frac{\sqrt{3}}{2}\hat{\mathbf{x}} - \frac{1}{2}\hat{\mathbf{y}}, -\frac{\sqrt{3}}{2}\hat{\mathbf{x}} - \frac{1}{2}\hat{\mathbf{y}}\right\}. \tag{2.5}$$

In order to write the free energy as a sum over a fixed number of particles, we consider a homogeneous system and a bulk chemical potential which, together with $V$, determines the lattice spacing and fixes the density of particles.

### A. Symmetric particle-wall potentials

Upon expanding $\bar{\Omega} \equiv \Omega/A$ about the height $f$=0 and the in-plane displacement $\mathbf{u} = 0$, and using $\mu(a)$ calculated to the appropriate order of further-neighbor interactions, the nearest-neighbor free-energy density becomes

$$\begin{aligned}\bar{\Omega} = \text{const} &+ \frac{K_2}{A}\sum_{\mathbf{x}}\sum_{i=1}^{3}|\mathbf{e}_i \cdot \Delta_i \mathbf{u}(\mathbf{x})|^2 + \frac{K_1}{2A}\sum_{\mathbf{x}}\sum_{i=1}^{3}\left[|\Delta_i \mathbf{u}(\mathbf{x})|^2 + |\Delta_i f(\mathbf{x})|^2\right] \\ &- \frac{K_2}{2aA}\sum_{\mathbf{x}}\sum_{i=1}^{3}(\mathbf{e}_i \cdot \Delta_i \mathbf{u}(\mathbf{x}))|\Delta_i f(\mathbf{x})|^2 + \frac{K_2}{8a^2A}\sum_{\mathbf{x}}\sum_{i=1}^{3}|\Delta_i f(\mathbf{x})|^4 \\ &+ \frac{K_3}{48a^4A}\sum_{\mathbf{x}}\sum_{i=1}^{3}|\Delta_i f(\mathbf{x})|^6 + \cdots + V(f,h)\end{aligned} \tag{2.6}$$

with

$$V(f,h) = \sum_{\mathbf{x}}\left(\frac{r}{2}f^2(\mathbf{x}) + uf^4(\mathbf{x}) + vf^6(\mathbf{x}) + \cdots\right) \tag{2.7}$$

and

$$A = \frac{A_0}{3N}\sum_{\mathbf{x}}\sum_{i=1}^{3}\left[1 - \frac{2}{a}(\mathbf{e}_i^1 \cdot \Delta_i^1 \mathbf{u}) + \frac{1}{a^2}|\Delta_i^1 \mathbf{u}|^2 - \frac{8}{3a^2}(\mathbf{e}_i^1 \cdot \Delta_i^1 \mathbf{u})^2 + \frac{8}{3a^2}(\mathbf{e}_i^1 \cdot \Delta_i^1 \mathbf{u})(\mathbf{e}_{i+1}^1 \cdot \Delta_{i+1}^1 \mathbf{u})\right], \tag{2.8}$$

the projected area of $N$ colloid particles to second order in $\mathbf{u}$. In these and subsequent equations, objects with direction indices $\{i\}$ are cyclic: $O_i \equiv O_{i+3}$. The notation $\mathbf{a}_i^1 \equiv \mathbf{a}_i$ and $K_{1,2,3}^1 \equiv K_{1,2,3}$ corresponding to a nearest-neighbor approximation are used. In going from (2.4) to (2.6), terms linear in $\mathbf{u}$ have been canceled by $\mu(a)/A$. For further neighbors, we use the notation $\Delta_i^n \phi \equiv \phi(\mathbf{x}) - \phi(\mathbf{x} + \mathbf{a}_i^n)$. To include the effects of the $n$th nearest-neighbor spheres at in-plane distance $a_n$, additional terms such as $\frac{K_1^{(n)}}{2A}\sum_{i,\mathbf{x}}|\Delta_i^{(n)} f(\mathbf{x})|^2$ must be added to Eq. (2.6). The constant term will be omitted in future equations.

The parameters $K_1^n, K_2^n$, and $K_3^n$ are completely defined by the effective microscopic particle-particle interactions,

$$K_1^{(n)} \equiv \frac{1}{a_n}\frac{\partial U}{\partial \xi}(a_n), \tag{2.9}$$

$$K_2^{(n)} \equiv \frac{\partial^2 U}{\partial \xi^2}(a_n) - K_1^{(n)}, \tag{2.10}$$

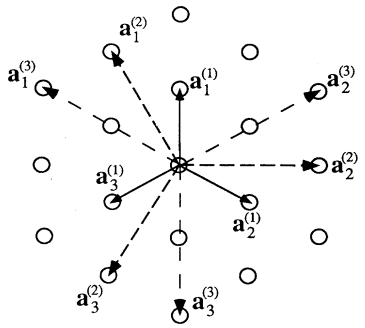


FIG. 2. Vectors indexing coordination shells for a triangular lattice. $|\mathbf{a}^{(1)}| = a$; $|\mathbf{a}^{(2)}| = \sqrt{3}a$, $|\mathbf{a}^{(2)}| = \sqrt{3}a, \ldots$.

$$K_3^{(n)} \equiv \frac{a_n}{3}\frac{\partial^3 U}{\partial \xi^3}(a_n) - K_2^{(n)}. \tag{2.11}$$

The expression for $V$ is a Taylor expansion of the total particle-plate potential. In the absence of an external field and using identical confining plates, the function $V(f)$ is symmetric and its expansion contains only even powers of $f$. The terms in Eq. (2.6) contain the contributions from competing interactions. For repulsive particle-particle interactions $K_1^n < 0$; consequently the energy density maximizes $|\Delta_i f(\mathbf{x})|^2$ throughout the sample. However, when repulsion from the walls, $V(h, f)$, is strong enough, buckling is prevented.

### B. Asymmetric potentials

Thus far, we have considered only symmetric particle-wall potentials in the absence of external perturbations. In general, however, an external field may couple linearly to the height function $f$,

$$V_{\text{ext}}(f) = \lambda \sum_x f(\mathbf{x}). \tag{2.12}$$

These perturbations may result from the effects of gravity or plate material asymmetry. An externally applied electric field would couple in this manner but would also induce dipoles resulting in an additional repulsive force between the particles. The total wall-particle potential becomes

$$V(f,h) = \frac{r(h)}{2}f^2 + uf^4 + vf^6 + \cdots + \lambda f. \tag{2.13}$$

In mean field theory, this linear term shifts the minimum of each particle from $f = 0$ to $\bar{f}$ where $\bar{f}$ is found by minimizing (2.13) with respect to $f$. Keeping terms only to fourth order in $f$, we find

$$\bar{f} \simeq \frac{(3u)^{1/3}\left[\sqrt{9\lambda^2 + r^3/3u} - 3\lambda\right]^{2/3} - r}{2(3u)^{2/3}\left[\sqrt{9\lambda^2 + r^3/3u} - 3\lambda\right]^{1/3}}. \tag{2.14}$$

Reexpansion of (2.2) about $\bar{f}$ yields [15]

$$V(f,h) \simeq \text{const} + \sum_{\mathbf{x}}\left(\frac{\bar{r}}{2}\eta(\mathbf{x})^2 + \hat{\lambda}\eta^3(\mathbf{x}) + u\eta^4(\mathbf{x}) + \cdots\right). \tag{2.15}$$

Here, $\eta = f - \bar{f}$, and the new expansion parameters are related to the ones in symmetric potential case by

$$\bar{r} = r + 12u\bar{f}^2, \tag{2.16}$$

$$\bar{\lambda} = 4u\bar{f}. \tag{2.17}$$

When asymmetry is taken into account, (2.6) is modified by replacing $f$ with $\eta$, $r$ by $\bar{r}$, and adding the term $\bar{\lambda}\eta^3$. This cubic term changes the nature of the transitions.

## III. STABILITY ANALYSIS

We now examine the region of validity of the free energy (2.6). In particular, we determine when and if phonons in the $\mathbf{u}$ or $f$ fields become unstable or "soft." This analysis is most convenient in Fourier space. We define the Fourier modes,

$$\mathbf{u}(\mathbf{x}) = \sum_{\mathbf{k}} \mathbf{u}(\mathbf{k})\exp(i\mathbf{k}\cdot\mathbf{x}) \tag{3.1}$$

and

$$f(\mathbf{x}) = \sum_{\mathbf{k}} f(\mathbf{k})\exp(i\mathbf{k}\cdot\mathbf{x}) \tag{3.2}$$

where $f(\mathbf{k}) = f^*(-\mathbf{k})$ and $\mathbf{u}(\mathbf{k}) = \mathbf{u}^*(-\mathbf{k})$ since the displacements are real. When periodic boundary conditions apply, the sums are over wave vectors spaced $2\pi/L$ apart where $L$ is the linear dimension of of the $N$-particle system.

To quadratic order, the free energy becomes

$$\bar{\Omega} \equiv \frac{1}{2NA}\sum_{\mathbf{G},\mathbf{k}}\left[r(h) + \sum_n D_n(\mathbf{k})\right] f(\mathbf{k})f(\mathbf{G}-\mathbf{k}) + \frac{1}{2NA}\sum_{\mathbf{G},\mathbf{k}}\mathbf{u}(\mathbf{k})\cdot\left(\sum_n \mathbf{M}_n(\mathbf{k})\right)\cdot\mathbf{u}(\mathbf{G}-\mathbf{k}). \tag{3.3}$$

In (3.3), we keep only the pieces quadratic in $\mathbf{u}$ which are not surface terms as they do not affect the eigenvalues $\omega^2(\mathbf{k})$ of this dynamical matrix. The $\mathbf{G}$ are reciprocal lattice vectors with $|\mathbf{G}| = 4\pi/\sqrt{3}a$.

In this paper, we consider buckling instabilities in out-of-plane modes with the modes in $\mathbf{u}$ remaining stable. For the in-plane phonons, stability requires that the eigenvalues of the dynamical matrix, $\sum_n \mathbf{M}_n(\mathbf{k})$, be real and positive. In the nearest-neighbor approximation,

$$\mathbf{M}_1(\mathbf{k}) = \begin{pmatrix} D_1(\mathbf{k}) + \frac{3}{2}K_2(2 - \cos\mathbf{k}\cdot\mathbf{a}_2 - \cos\mathbf{k}\cdot\mathbf{a}_3) & \frac{\sqrt{3}}{2}K_2(\cos\mathbf{k}\cdot\mathbf{a}_2 - \cos\mathbf{k}\cdot\mathbf{a}_3) \\ \frac{\sqrt{3}}{2}K_2(\cos\mathbf{k}\cdot\mathbf{a}_2 - \cos\mathbf{k}\cdot\mathbf{a}_3) & D_1(\mathbf{k}) + \frac{K_2}{2}(6 - 4\cos\mathbf{k}\cdot\mathbf{a}_1 - \cos\mathbf{k}\cdot\mathbf{a}_2 - \cos\mathbf{k}\cdot\mathbf{a}_3) \end{pmatrix}, \quad (3.4)$$

where

$$D_1(\mathbf{k}) = 2K_1(3 - \cos\mathbf{k}\cdot\mathbf{a}_1 - \cos\mathbf{k}\cdot\mathbf{a}_2 - \cos\mathbf{k}\cdot\mathbf{a}_3). \quad (3.5)$$

We find that the all eigenvalues of $\mathbf{M}_1(\mathbf{k})$ are always real and are positive provided

$$K_1 + \frac{K_2}{2} > 0 \quad (3.6)$$

and

$$\left(\frac{1}{K_2} + \frac{1}{2K_1}\right)^2 > \frac{1}{D_1^2(\mathbf{k})}\sum_{i=1}^{3}\left(\cos^2\mathbf{k}\cdot\mathbf{a}_i - \cos\mathbf{k}\cdot\mathbf{a}_i\,\cos\mathbf{k}\cdot\mathbf{a}_{i+1}\right) \quad (3.7)$$

with $\mathbf{a}_i \equiv \mathbf{a}_{i+3}$. The criterion (3.6) is satisfied with repulsive potentials in general. In the first Brillouin zone, the right hand side of (3.7) varies between 0 and $K_1^{-2}/16$. Therefore in the nearest-neighbor approximation, in-plane phonons are stable provided

$$\left(K_1 + \frac{K_2}{4}\right)\left(K_1 + \frac{3K_2}{4}\right) > 0. \quad (3.8)$$

This is just a more stringent version of (3.6) and satisfied by potentials which are repulsive and short ranged consistent with the nearest-neighbor approximation.

Now, we find instabilities in the magnitude of $f(\mathbf{k})$ and assume that the phase of the displacement functions has been fixed to minimize the free energy. The dependence of the corrugations on the phase of $f$ will be discussed later. Provided (3.7) holds, we can consider only the instabilities in the transverse modes, $f$. Here, we require

$$\omega^2(\mathbf{k}) \equiv r(h) + \sum_n D_n(\mathbf{k}) \leq 0 \quad (3.9)$$

for *instability* of the $\mathbf{k}$th mode of $f(\mathbf{k})$. As the spacing between the plates increases, the compressional forces balancing the inward forces from the colloid bath and $r(h)$ decrease. The points at which the criterion (3.9) is first satisfied selects the first modes to soften. An estimate of the critical spacing $h_c$ can be made by solving $r(h_c) \simeq -\sum_n D_n(\mathbf{k}_c)$.

In the nearest-neighbor truncation, $r(h) = -D_1(\mathbf{k})$; the values of $\mathbf{k}_c$ that satisfy this relation for the largest value of $r(h)$ are at the corners of a hexagonal Brillouin zone shown in Figs. 3(a) and 3(b). Thus, as $r(h)$ is decreased the first out-of-plane corrugations of the colloidal array will occur at these wave vectors. When further neighbors are considered, $\mathbf{k}_c$ can shift to the edges of the Brillouin zone. The location of these first instabilities depends on the relative sizes of $K_1^{(n)}$. When only nearest neighbor are included, only corner instabilities arise. In the next-nearest-neighbor truncation, the first unstable modes can occur at the zone edges when

$$|K_1^{(2)}| > \frac{1}{8}|K_1| \quad (3.10)$$

as shown in Figs. 3(a) and 3(c). With repulsive and reasonably short ranged potentials (such that $K_1^{(n>2)} \approx 0$), the corner and edge instabilities are always the first to

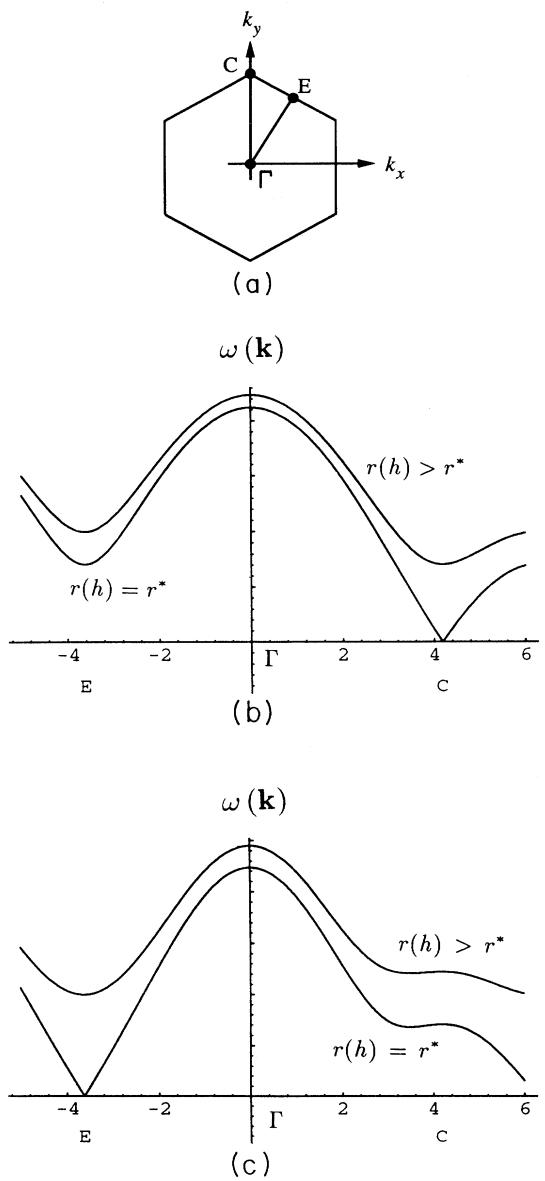


FIG. 3. The function $\omega^2(\mathbf{k}) = r(h) + D_1(\mathbf{k}) + D_2(\mathbf{k})$ slightly above and exactly at the transition. The first Brillouin zone is shown in (a). Zeros first occur at a corner (b). When $|K_1^{(2)}| > \frac{1}{8}|K_1|$, an edge instability arises (c).

occur. Further-neighbor interactions can shift the instabilities away from the corners or edges only if they are nearly as strong as the nearest-neighbor potentials. We will restrict this discussion to the corner and edge type of instabilities. The real-space structures of these corrugations are depicted in Fig. 4.

Since three pairs of corner instability points are connected via reciprocal lattice vectors, the height function $f$ is the real part of a one-component complex function. The edge modes can be represented by a three-component function. The sums over critical wave vectors $\mathbf{k}_c$ are thus restricted to the stars of $\pm\mathbf{k}_0$ and $\mathbf{q}_i (i = 1,2,3)$ belonging to the symmetries of the corner and edge instabilities, respectively,

$$\mathbf{k}_0 \equiv \pm\frac{4\pi}{3a}\hat{\mathbf{y}}, \tag{3.11}$$

$$\mathbf{q}_1 \equiv \frac{2\pi}{\sqrt{3}a}\hat{\mathbf{x}},$$

$$\mathbf{q}_2 \equiv \frac{-\pi}{\sqrt{3}a}\hat{\mathbf{x}} - \frac{\pi}{a}\hat{\mathbf{y}},$$

$$\mathbf{q}_3 \equiv \frac{-\pi}{\sqrt{3}a}\hat{\mathbf{x}} + \frac{\pi}{a}\hat{\mathbf{y}}. \tag{3.12}$$

These two sets of unstable modes transform as particular irreducible representations of the space group of the lattice. Since the height function can be written as linear combinations of the basis functions of one of these two irreducible representations (excluding the unit representation), a continuous transition into these ordered structures is possible if no cubic invariant in the free energy exists [12,16]. This Landau rule is not exact in two dimensions because fluctuations can lead to continuous transitions even when the cubic term is present [15,21]. Landau theory nevertheless plays an essential role in determining the *universality class* of the transition. The functions $f(\pm\mathbf{k}_0)$ and $f(\mathbf{q}_i)$ are identified with $d$ component order parameters where $d = 2,3$ are the dimensionalities of the irreducible representations [16,17].

When unstable modes with wave vectors at zone boundaries occur, the energy will depend on the phase of $f$. For example, with $\mathbf{k}$ and $-\mathbf{k}$ pointing to the midpoint of an edge of the Brillouin zone boundary, careful enumeration of the sums over wave vectors of the reduced group, or star, leads to a quadratic term $\propto \frac{1}{2}(f_k f_k + c.c.)$.

The free energy without phase terms is correct for wave vectors such that $\mathbf{k}+\mathbf{k}' \neq \mathbf{G}$ and is sometimes termed the "incommensurate" free energy. However, when the relevant wave vector is a rational fraction of the reciprocal lattice vector, the phase variable enters and a "commensurate" free energy is obtained [13]. Since the functions $\sum_n D_n(\mathbf{k})$ for $n \leq 3$ appear to have stable extrema only at corners or midpoints of edges, the commensurate wave vectors (3.11) and (3.12) are the most important. Thus we expect the system to order directly into a corrugation with a commensurate wave vector.

We now derive these commensurate energies. Since the energy was a sum over discrete lattice sites, the expression (3.3) contains sums over $\mathbf{G}$. Thus, at the boundaries of the Brillouin zone, certain wave vectors can participate in the "umklapp processes" shown in Fig. 5. It is these terms that generate $\phi$-dependent terms in the energy that lock the phase. The phase dependence can be incorporated by generalizing the order parameter, and allowing for slow spatial undulations in both the phase and amplitude,

$$f(\mathbf{k}) = f_{\mathbf{k}}(x)e^{i\phi_{\mathbf{k}}(x)}, \tag{3.13}$$

where $f_{\mathbf{k}}(x)$ and $\phi_{\mathbf{k}}(x)$ are real positive functions. The procedure we follow is first fixing the amplitude and phase of the order parameters, expressing the energy in terms of these variables, then allowing slow spatial modulations within the sample.

At $\mathbf{k}_c = \pm\mathbf{k}_0$ [the corner instabilities shown in Fig. 3(a)], the nearest-neighbor $\mathbf{u}(\mathbf{k})$ independent part of the commensurate free energy becomes

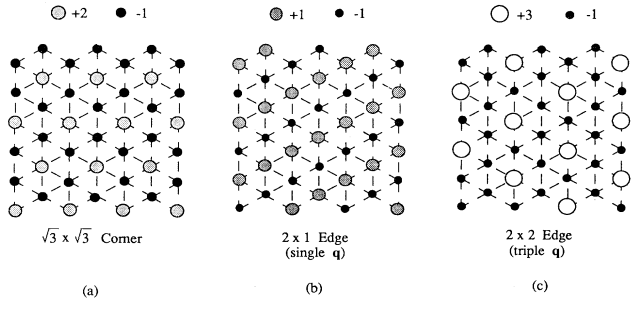


FIG. 4. Minimum energy structures with out-of-plane displacements indicated. (a) $\sqrt{3} \times \sqrt{3}$ corrugation. (b) $2 \times 1$ structure. (c) $2 \times 2$ structure. Note that not all particles have equal displacement magnitudes; however, $\sum_{\mathbf{x}} f(\mathbf{x}) = 0$.

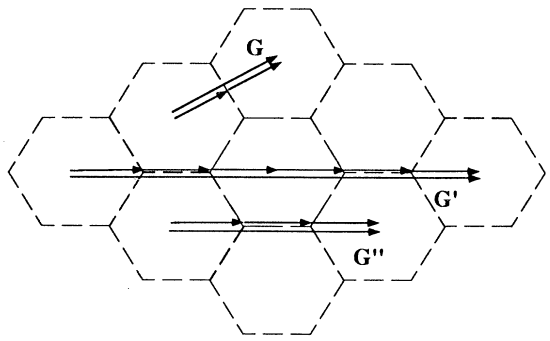


FIG. 5. "umklapp" processes for corner and edge instabilities. In the absence of asymmetry, $\mathbf{G} = 2\mathbf{q}_i$ for the edge modes: the phases are fixed by the first quadratic term. For the corner instabilities, $\mathbf{G}' = 6\mathbf{k}_0$ is the first umklapp term. When a cubic term exists, a lower order umklapp, $3\mathbf{k}_0 = \mathbf{G}''$, appears.

$$\bar{\Omega} = \frac{1}{A}\left[r(h) + 9K_1\right]|f(\mathbf{k}_0)|^2 + \frac{1}{A}\left(6u + \frac{81K_2}{4a^2}\right)|f(\mathbf{k}_0)|^4 + \frac{1}{A}\left(20v + \frac{243K_3}{8a^4}\right)|f(\mathbf{k}_0)|^6 + \frac{1}{A}\left(2v - \frac{81K_3}{8a^4}\right)\cos(6\phi)|f(\mathbf{k}_0)|^6 + \cdots. \tag{3.14}$$

Since $2v - 81K_3/8a^4 > 0$, the six phases minimizing (3.14) for the $\sqrt{3} \times \sqrt{3}$ state are $\{\phi_m\} = \{(2m+1)\pi/6,\ m = 0, ..., 5\}$. They represent three equivalent states generated by translations in three directions. This degeneracy in each of these states is doubled by the inversion $f(\mathbf{k}_0) \to -f(\mathbf{k}_0)$.

For edge wave vectors the quadratic terms fix the phase $\phi$ of the displacement fields at $\phi = m\pi$, provided higher order terms are sufficient to stabilize the energy. For these critical modes, $\mathbf{k}_c = \mathbf{q}_i$ $(i = 1, 2, 3)$, we have

$$\bar{\Omega} = \frac{1}{A}\left(4K_1 + 4K_1^{(2)} + \frac{r(h)}{2}\right)\sum_{i=1}^{3}(1 + \cos 2\phi_i)|f_i|^2 + \left(\frac{u}{A} + \frac{4K_2}{a^2A} + \frac{4K_2^{(2)}}{3a^2A}\right)\sum_{i=1}^{3}|f_i|^4\cos 4\phi_i + \left(\frac{u}{A} + \frac{2K_2}{a^2A} + \frac{2K_2^{(2)}}{3a^2A}\right)\sum_{i=1}^{3}\left\{3|f_i|^2|f_{i+1}|^2\cos[2(\phi_i + \phi_{i+1})] + 3|f_i|^2(|f_{i-1}|^2 + |f_{i+1}|^2)\cos 2\phi_i\right\} + \cdots, \tag{3.15}$$

where we have set $f_i \equiv f(\mathbf{q}_i)$ and $\phi_i \equiv \phi(\mathbf{q}_i)$. In this case the quadratic term selects the phase. For $4K_1 + 4K_1^{(2)} + r/2 < 0, \phi = m\pi$ and the quadratic coefficient in (3.15) at this phase is $8K_1 + 8K_1^{(2)} + r(h)$. Comparing (3.14) with (3.15) leads to the condition (3.12) for edge instabilities.

When edge instabilities and phases lock as described above, the order parameter still contains three independent real components $\{|f_i|\}$ corresponding to three equivalent directions for the corrugation. In principle, the quadratic couplings in Eq. (3.15) could select a "triple-**q**" structure [see Fig. 4(c)], in which all three components order simultaneously. However, in the symmetric wall potential case, the ordered state has a configuration with all the weight in one of these components which is spontaneously chosen by the system. This "single-**q**" state minimizes the free energy for symmetric wall potentials and is depicted in Fig. 4(b). This resembles an observed mazelike pattern [9,18] and can be an intermediate structure in the transition to the 2□ phase. However, we do not expect antiferromagnetic Ising behavior (see below) as suggested by Ogawa [18]. For the free energy (3.15), a 3-**q** state, where all the $|f_i|$ are equal, is favored only in the presence of asymmetry in $V(f)$

## IV. CORRESPONDENCE OF FREE ENERGY TO CONTINUUM STATISTICAL MODELS

We now explicitly allow the order parameter to acquire a slowly spatially varying modulation, as defined in (3.13). This is equivalent to expanding **k**-dependent quadratic coefficients $D_1(\mathbf{k})$ about $\mathbf{k} \simeq \mathbf{k}_0$. With the notation $f_0(x) \equiv f_{\mathbf{k}_0}(x)$ and $\phi_0(x) \equiv \phi_{\mathbf{k}_0}(x)$, the nearest-neighbor free energy in position space becomes

$$\bar{\Omega} = \frac{3a^2|K_1|}{4A}|\nabla f_0(x)|^2 + \frac{1}{A}\left[9K_1 + r(h)\right]f_0^2(x) + \frac{1}{A}\left(6u + \frac{81}{4a^2}K_2\right)f_0^4(x) + \frac{1}{A}\left(20v + \frac{243}{8a^4}K_3\right)f_0^6(x) + \frac{1}{A}\left(2v - \frac{81}{8a^4}K_3\right)\cos\left[6\phi_0(x)\right]f_0^6(x) + \cdots. \tag{4.1}$$

At a fixed amplitude which minimizes $f_0$, the expression describing the energetics of the phase variable becomes

$$\bar{\Omega} = \frac{3a^2|K_1|}{4A}|\nabla\phi_0(x)|^2 f_0^2 + \frac{1}{A}\left(2v - \frac{81}{8a^4}K_3\right)f_0^6\cos[6\phi_0(x)] + \cdots. \tag{4.2}$$

This expression has the form of the 2D $X$-$Y$ model with sixfold anisotropy as discussed by José and others [14,19]. This model is expected to order in two steps with an intermediate region of continuously varying exponents as the parameters are varied.

When asymmetry exists,

$$\bar{\Omega} = \frac{3a^2|K_1|}{4A}|\nabla\phi_0(x)|^2\eta_0^2 + \frac{2}{A}\bar{\lambda}\eta_0^3\cos\left[3\phi_0(x)\right] + \cdots. \tag{4.3}$$

Here, the largest phase locking term is proportional to $\eta_0^3\cos 3\phi_0$ To minimize the energy, the phases prefer the values $\phi_0 = \{\pm\frac{\pi}{3}, \pi\}$ when $\bar{\lambda} > 0$ and $\{0, \pm\frac{2\pi}{3}\}$ when $\bar{\lambda} < 0$. This Hamiltonian is identical to that of the continuum 3-state Potts model [20]. The behavior of this Hamiltonian has been studied extensively [20–23]; a *continuous* transition is possible, and the critical exponents are known [21].

When the edge modes buckle, there exist two cases. If a 1-**q** state is favored, any one of three directions is selected,

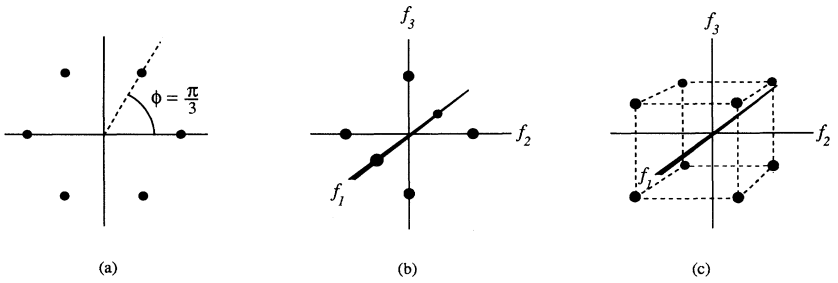


FIG. 6. Order-parameter-space representation of model Hamiltonians. Energy minima are shown by filled circles. (a) The $X$-$Y$ model with sixfold anisotropy when corner instabilities arise. (b) Heisenberg model when a 1-**q** state is chosen within the edge instability subspace. (c) Heisenberg model when "cubic" interactions dominate, $(3-\mathbf{q})$.

each with two preferred phases $\phi$. These conditions are described by a Heisenberg model with quartic couplings proportional to $\left(\sum_{i=1}^{3}|f_i|^2\right)^2$ and $\sum_{i=1}^{3}|f_i|^4$. The exact critical behavior of this model in two dimensions is, to the best of our knowledge, as yet unknown.

In fact, for the particular Hamiltonian at hand, the 3-**q** state is energetically preferred over the 1-**q** one only when appreciable symmetry breaking interactions (gravity or asymmetric plates) are present. The term

$$\bar{\lambda}\sum_{i=1}^{3}\eta_1\eta_2\eta_3\cos(\phi_i+\phi_{i+1}-\phi_{i+2}) \tag{4.4}$$

favors the 3-**q** or $2\times 2$ state shown in Fig. 4(c); energy configurations with any $\eta_i = 0$ will be unaffected. In the presence of such a term, the degeneracy in phases of the 3-**q** structure is halved. Now the sets $\{\phi_i\} = \{(\pi,\pi,\pi),(0,0,\pi),(0,\pi,0),(\pi,0,0)\}$ and $\{(0,0,0),(\pi,\pi,0),(\pi,0,\pi),(0,\pi,\pi)\}$ are selected when $\bar{\lambda} > 0$ and $\bar{\lambda} < 0$, respectively. A 4-state Potts model (which also has a continuous transition in $d = 2$) is recovered in this case [17,21,24]. Of course, as $r(h)$ is decreased further, discontinuous transitions from the 3-**q** to 1-**q** corrugations are possible.

The minimum energy configurations in order-parameter space are shown in Fig. 6. In general, a state described by an equally weighted superposition of directions, the 3-**q** state, has eight possible combinations of the three phases associated with each order-parameter component that minimize the energy, as shown in Fig. 6(c). The $\sqrt{3}\times\sqrt{3}$ corner instability is represented by Fig. 6(a) and Fig. 7(a) for the symmetric and asymmetric cases, respectively. For the free energies derived from our microscopic model, the situation depicted in Fig. 6(c) does not occur since in the absence of a symmetry breaking term, the 1-**q** state [Fig. 6(b)] is always preferred.

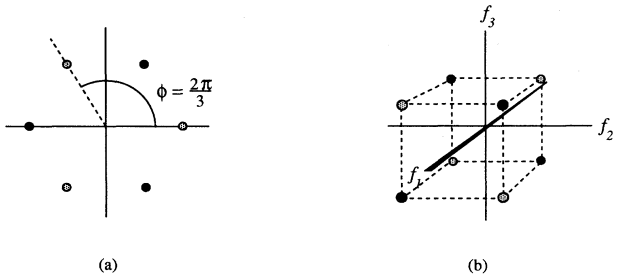


FIG. 7. Order-parameter representation with asymmetry. (a) 3-state Potts. (b) Heisenberg model with cubic interactions. The light and dark points refer to opposite signs of the asymmetry parameter $\lambda$.

## V. EXPERIMENTAL CONSEQUENCES

In this section, we briefly examine the experimental signatures expected for each of the buckled structures above. To begin, we must have a rough description of the interaction parameters. The simplest DVLO type potentials for the sphere-sphere and sphere-wall interactions in the charge stabilized limit are the Yukawa and exponential forms, respectively,

$$U(r) = \frac{U_0}{r}e^{-\kappa r}, \tag{5.1}$$

$$V(f,h) = V_0 e^{-\kappa(h/2-f)} + V_0 e^{-\kappa(h/2+f)}. \tag{5.2}$$

In the experiments of Murray and co-workers [6], a layer of $0.3-\mu m$ poly(styrene) sulfonate spheres was confined in a gap $h \sim 3\mu$m. To stabilize the structures, low ionic strength solvents with $\kappa a \sim 0.05$, where $\kappa$ is the Debye screening length, were used. With these estimates we find $|K_i| \sim 1\times 10^{-3}$erg/cm$^2$, $r(h) \sim 0.1$ erg/cm$^2$, and $u(h) \sim 1$ erg/cm$^4$. Interactions of the form (5.2) make $r$ and $u$ very sensitive to the gap spacing $h$ and very small wedge angles are probably needed to study these transitions in detail. Although our analysis has neglected the equilibrium thermal fluctuations of the spheres in solution, it will correctly identify the symmetry or "universality class" of the various transitions. Thermal fluctuations will change the detailed predictions of mean field theory whenever the mean square fluctuations of the order-parameter amplitude exceeds its equilibrium value.

Asymmetry effects can be described by the additional term (2.12). If the external field of concern is gravity, $\lambda = v_0(\rho_c-\rho_0)g$, where $v_0$ is the volume of each particle and $\rho_c$ and $\rho_0$ are the densities of the colloid and suspending fluid, respectively. For poly(styrene) spheres, $\lambda \simeq 7\times$

$10^{-13}$ erg/cm.

An estimate of the relative displacement of the entire layer from the center of the gap using the values in (2.14) gives $|\bar{f}/h| \sim 1 \times 10^{-8}$ which is truly negligible. Another measure of the degree of asymmetry is the change in the critical value $r^*(h)$ where the magnitude $f_{\mathbf{k}}$ first becomes nonzero. At a corner instability ($\sqrt{3} \times \sqrt{3}$), for $\lambda << K_1^2/u$,

$$r_\lambda^* - r_0^* \equiv \delta r^* \simeq \frac{4\lambda^2}{81K_1^2}\left[\frac{4a^2u}{24ua^2 + 81K_2} - 3\right]. \quad (5.3)$$

Since $K_2 > 0$ and $\bar{f}$ depends on $r(h)$, the critical value $r^*(h)$ is *lowered* by the presence of $\lambda$, i.e., a larger $h^*$ is required to buckle the lattice.

Given that the conditions for equilibrium ordering are met, there are essentially two methods currently used to probe these structures: direct video imaging and diffraction. When thermal fluctuations are strong, laser light diffraction patterns can be analyzed to elucidate average structural features.

For monochromatic light incident on the layers (the plates are made transparent), diffraction peaks are expected at wave-vector transfers equal to the critical wave vectors [(3.11) and (3.12)]. The $\sqrt{3} \times \sqrt{3}$ structure is defined by a primitive cell with three times the area of the original, undistorted lattice. A three point basis is also superimposed. The static, zero temperature structure factor for point, single scatterers in this case is

$$\delta(\mathbf{k}_\perp, \mathbf{G})\delta(-\mathbf{k}_\perp, \mathbf{G}')\Big\{2 + 2\cos(\mathbf{k}\cdot\mathbf{e}_1 + k_z z_0) + 2\cos[\mathbf{k}\cdot(\mathbf{e}_1 + \mathbf{e}_2) + k_z z_0)]\Big\} \quad (5.4)$$

where the 2D reciprocal lattice corresponding to the larger hexagonal lattice is

$$\{\mathbf{G}\} = \left(\frac{n4\pi}{3a}\hat{\mathbf{y}}, \frac{m4\pi}{3a}\left(\frac{\sqrt{3}}{2}\hat{\mathbf{x}} + \frac{1}{2}\hat{\mathbf{y}}\right)\right) \quad (5.5)$$

and $z_0$ is the spacing between the two flat lattices, $z_0 = \frac{3}{2} f_{\mathbf{k_c}}$. In a $\sqrt{3} \times \sqrt{3}$ structure, in addition to the six spots expected from the original triangular lattice, we would see six additional first order peaks at smaller wave-vector transfers and rotated by 30° provided $z_0$ is large enough. This pattern is in marked contrast to the asymmetric, three-spot pattern seen in diffraction from a $2\triangle$ superlattice. We note that *all* diffraction spots in two dimensions are algebraic singularities [14], rather than true $\delta$-function Bragg peaks.

The $2\times2$ structure has even a larger primitive cell and a four-point basis. The six diffraction pattern peaks would be even closer to the origin than in the $\sqrt{3}\times\sqrt{3}$ structure and would not be rotated with respect to the six original peaks. A pattern consisting of four spots rectangularly positioned would be an indication of a $2 \times 2$ superlattice. A similar square pattern develops when the ordering is $2\square$. It would be interesting see how these patterns evolve as $r(h)$ is decreased.

In addition to diffraction patterns, video imaging of the colloidal crystal may reveal the out-of-plane buckling and the concomitant in-plane lattice distortions. The in-plane contractions are due to the $\mathbf{e_i}\cdot\Delta_i\mathbf{u}|\Delta_i f|^2$ terms in (2.6) which we have neglected. To predict any effects in the lattice spacing as buckling occurs, we minimize the energy density $\bar{\Omega}$ with respect to the $\Delta_i\mathbf{u}$ associated with the specific corrugations in Fig. 4. The $\Delta_i\mathbf{u}$ used are the $\mathbf{k} = \mathbf{0}$ modes expected on symmetry grounds for each of the structures. A $\sqrt{3}\times\sqrt{3}$ buckling is expected to induce a symmetric contraction of magnitude,

$$\frac{\Delta a}{a} \simeq \frac{3}{4a^2}\langle f^2(\mathbf{k}_0)\rangle. \quad (5.6)$$

The contractions depend on $\langle f_{\mathbf{k}}^2\rangle$, which in turn behaves according to the relevant model near the transition with an $|r - r^*|^{1-\alpha}$ energylike singularity. Similar expressions hold for the other buckled structures. Direct observation of lattice contractions may reveal the nature of the buckling transition even if the predicted extra spots are blurred by thermal fluctuations. It is not clear how strongly the in-plane displacements are coupled to the buckling at larger amplitudes. For instance, individual fluctuations in $f(\mathbf{x})$ of the charge stabilized particles can induce a fluctuating dipole in the $\hat{\mathbf{z}}$ direction which would contribute a net repulsion between the particles tending to expand the lattice. Furthermore, tuning of the ionic strength or temperature can vary the range of particle-particle interactions thus determining whether corner or edge instabilities occur.

## VI. SUMMARY

Stability analysis has shown that the buckling of a layer of confined repelling particles results from the competition between a bulk compressional force derived from a chemical potential and a confining wall force derived from a repulsive particle-wall potential. We have found that the unstable modes have wave vectors $\mathbf{k_c}$ at the midpoint of edges and at the corners of the Brillouin zone boundaries. These instabilities correspond to the $2 \times 1$ or $2 \times 2$ and the $\sqrt{3} \times \sqrt{3}$ structures, respectively. In this analysis, the edge instabilities arose only when further-neighbor interactions were considered. The additional restriction (3.9) was imposed for the in-plane phonons to remain stable.

The symmetry allowed buckled states have basis functions belonging to irreducible representations of the point group. Furthermore, an expansion of the order parameter coefficients in the wave-vector index $\mathbf{k}$ yields minima at $\mathbf{k_c}$. Despite the Landau rule prohibiting a continuous transition in the presence of gravity or plate asymmetry [12,16,13], we find that in this two-dimensional problem, second-order transitions may occur [17,23].

Provided we allow the order-parameter *phase* to be slowly space dependent, the free energy can be written in a continuum form. A striking feature is that these Hamiltonians allow for continuous transitions into the mentioned buckled structures, and are predicted to have

critical behavior corresponding to an $X$-$Y$ model with six-fold anisotropy for corner instabilities, and a Heisenberg model for an edge instability, the edge instability being relevant only when the repulsion from next nearest neighbors are included. Colloids between symmetrical confining plates may be the first experimentally realized nonmagnetic system which can be described by an $X$-$Y$ model with sixfold anisotropy. In general, the edge instability has critical behavior resembling that of a Heisenberg model with cubic interactions, although in this particular problem transitions to 3-**q** states are expected to occur only in the presence of asymmetry.

Asymmetry from the effects of gravity were found to be negligible. When asymmetry is expected to be important continuous transitions are not precluded by cubic invariants in the free energy. In these cases the Hamiltonians are in the 3-state and 4-state Potts universality classes for the corner and edge instabilities, respectively. It would be interesting to use differently treated upper and lower plates to enhance this asymmetry.

The structures enumerated above should be easily distinguished using light diffraction. We have estimated the structure factors and predicted the diffraction patterns that would result from these superlattices. It is also possible to obtain an estimate of the contraction in lattice spacing due to the buckling. This effect is described by the coupling term $(\mathbf{e}_i\Delta_i\mathbf{u})|\Delta_i f|^2$, in Eq. (2.6).

The main prediction of our theory lies in the analysis of the types of instabilities that may occur. We emphasize in conclusion that the precise mode of buckling and hence which type of phase transition occurs depend sensitively on the microscopic parameters in the theory.

*Note added in proof.* Warner and Hornreich have predicted instabilities in magnetic dipole lattices similar to the $2\times 1$ and $2\square$ states [M. Warner and R. M. Hornreich, J. Phys. A **18**, 2325 (1985)].

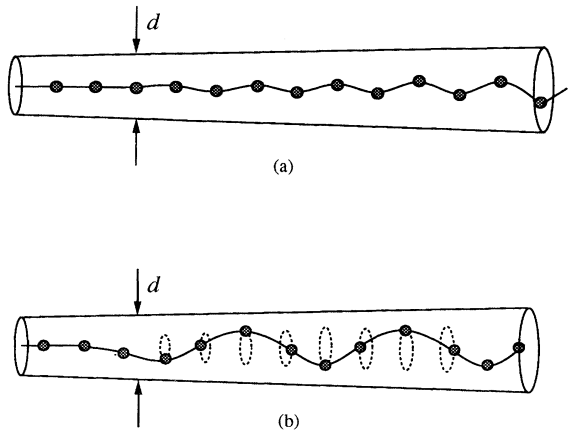


FIG. 8. A confining geometry of particles in a conical pore.

## ACKNOWLEDGMENTS

We are grateful to C. A. Murray, who brought this problem to our attention, and acknowledge helpful discussions as well with R. Seshadri, E. Domany, and J. Cardy. Support from the National Science Foundation through the Harvard Materials Research Laboratory Grant No. DMR-91-15491, and support for T.C. is gratefully acknowledged.

## APPENDIX A: ONE-DIMENSIONAL SYSTEM

In this section, we consider a related problem: a one-dimensional string of confined particles as shown in Fig. 8. For a line of regularly spaced nearest-neighbor repelling particles confined to a cylindrical tube, the free-energy expression equivalent to (2.6) is

$$\bar{\Omega}=\frac{(K_1+K_2)}{2L}\sum_i^N(u_{i+1}-u_i)^2+\frac{K_1}{2L}\sum_i^N|\vec{f}_{i+1}-\vec{f}_i|^2+\frac{K_2}{8a^2L}\sum_i^N\left(|\vec{f}_{i+1}-\vec{f}_i|^2\right)^2+\cdots$$
$$+\frac{1}{L}\sum_i^N\left(\frac{r}{2}|\vec{f}_i|^2+u(|\vec{f}_i|^2)^2+\cdots\right), \tag{A1}$$

where the length of $N$ particles is exactly

$$L=Na\left[1+\sum_i^N(u_{i+1}-u_i)\right]. \tag{A2}$$

Equation (A1) can be supplemented with similar terms to include further-neighbor interactions. The parameters $r(d)$ and $u(d)$ may be tuned by changing the pore diameter, or alternatively, by using a cone geometry. In contrast to the two-dimensional sheet, the in-line displacements $u_i$ are scalars and the out-of-line displacements $f_i$ are two component vectors. The harmonic free energy expression analogous to (3.3) is

$$M_n(k)=(K_2^{(n)}+K_1^{(n)})(2-2\cos nka) \tag{A3}$$

and

$$\sum_n D_n^{ij}(k) = \delta_{ij}\left[r(d) + \sum_n K_1^{(n)}(2 - 2\cos nka)\right], \tag{A4}$$

where $i, j$ label two orthogonal directions perpendicular to the tube axis.

The flat state in the nearest-neighbor case (A1) is unstable at wave vectors $k_c = \pm\pi/a$. The free-energy of a structure with an instablility at $k_c = \pi/a$ becomes

$$\bar{\Omega} = \left(\frac{2K_1}{L} + \frac{r(d)}{2L}\right)|\vec{f}(k_c)|^2 + \sum_{i=x,y}\left(\frac{r(d)}{2L}\cos 2\phi_i - \frac{K_1 a^2}{2L}|\nabla\phi_i|^2\right) f_i^2(k_c) + \cdots . \tag{A5}$$

In one dimension, however, the inclusion of the next-nearest-neighbor interactions pushes the first unstable modes inside the Brillouin zone to smaller $k_c$. The free energy of these longer wavelength modes will have higher order phase locking terms only if $k_c a/\pi$ is rational. Otherwise, the free energy resembles that of an isotropic $X$-$Y$ model,

$$\bar{\Omega} = \frac{1}{2L}\sum_{k_c,n} D_n(k_c)|\vec{f}(k_c)|^2 + \frac{1}{4L}\sum_{k_c,n}\sum_{i=x,y} n^2 a^2 f_i^2(k_c)\frac{\partial^2 D_n(k_c)}{\partial k^2}|\nabla\phi_i(x)|^2 + \cdots . \tag{A6}$$

Furthermore, each component of $\vec{f}_k$ contains a phase variable. In addition to the absolute phase, the phase difference $|\phi_x - \phi_y|$ also determines the structure. At zero temperature, the phases minimizing the nearest-neighbor approximation (A1) are $\phi_i = m\pi$ and the phase differences are 0 or $\pi$ corresponding to a linearly polarized wave as shown in Fig. 8(a).

If, from the inclusion of further neighbors, $k_c$ is incommensurate, or if the first phase locking term is very high order, the prefered phase differences $|\phi_x - \phi_y|$ vary continuously. For example, when $4|K_1^{(2)}| > |K_1|$ the next-nearest-neighbor truncation ($n = 1, 2$) yields

$$\cos k_c a = \frac{-K_1}{4K_1^{(2)}} \tag{A7}$$

and

$$\bar{\Omega} = \frac{1}{L}\left(r(d) + 2K_1 + 4K_1^{(2)} + \frac{K_1^2}{4K_1^{(2)}}\right)|\vec{f}(k_c)|^2 + \sum_{i=x,y} a^2 f_i^2(k_c)\left(\frac{K_1^2}{2K_1^{(2)}L} - \frac{8K_1^{(2)}}{L}\right)|\nabla\phi_i(x)|^2 + \cdots . \tag{A8}$$

The mean field structures available range from linearly polarized undulations ($|\phi_x - \phi_y| = m\pi$) to circularly polarized helices [$|\phi_x - \phi_y| = (2m+1)/2\pi$]. At low enough temperatures, these spontaneously chosen motifs may be observable.


[1] Robert S. Hunter, *Foundations of Colloid Science* (Oxford University Press, New York, 1989), Vol. II.

[2] S. P. Stoylov, *Colloid Electro-Optics, Theory, Techniques, Applications* (Academic Press, London, 1991).

[3] P. N. Pusey and W. van Megen, *Properties of Concentrated Suspensions of Slightly Soft Colloidal Spheres*, in *Physics of Complex and Supermolecular Fluids, An Exxon Monograph*, edited by S. A. Safran and N. A. Clark (Wiley, New York, 1987); J. Phys. (Paris) **44**, 285 (1983).

[4] K. Kremer, M. O. Robbins, and G. S. Grest, Phys. Rev. Lett. **57**, 2694 (1986); M. O. Robbins, K. Kremer, and G. S. Grest, J. Chem. Phys. **88**, 3286 (1988); E. J. Meijer and D. Krenkel, *ibid.* **94**, 2269 (1991).

[5] N. Ise, H. Matsuoka, K. Ito, and H. Yoshida, Faraday Discuss. Chem. Soc. **90**, 153 (1990).

[6] D. H. Van Winkle and C. A. Murray, Phys. Rev. A **34**, 562 (1986); C. A. Murray, in *Bond-Orientational Order in Condensed Matter Systems*, edited by K. J. Strandburg (Springer, New York, 1991).

[7] Pa. Pieranski, L. Strzelecki, and B. Pansu, Phys. Rev. Lett. **50**, 900 (1983).

[8] B. Pansu, P. Pieranski, and L. Strzelecki, J. Phys. (Paris) **44**, 531 (1983).

[9] T. Okubo, J. Chem. Phys. **95**, 3690 (1991).

[10] Pa. Pieranski, Phys. Rev. Lett. **45**, 569 (1980).

[11] B. Pansu, Pi. Pieranski, and Pa. Pieranski, J. Phys. (Paris) **45**, 331 (1983)

[12] A. D. Bruce and R. A. Cowley, *Structural Phase Transitions* (Taylor & Francis, LTD., London, 1981).

[13] J. C. Toledano and P. Toledano, *The Landau Theory of Phase Transitions: Applications to Structural, Incommensurate, Magnetic, and Liquid Crystal Systems* (World Scientific, Singapore, 1987).

[14] D. R. Nelson, in *Phase Transitions and Critical Phenomena*, edited by C. Domb and J. L. Lebowitz (Academic Press, New York, 1983), Vol. 7.

[15] S. Alexander and D. J. Amit, J. Phys. A **8**, 1988 (1975).

[16] L. D. Landau and E.M. Lifshitz, *Statistical Physics*, 3rd ed. (Pergamon Press, New York, 1980), Pt. I.

[17] E. Domany, M. Schick, J. S. Walker, and R. B. Griffiths, Phys. Rev. B **18**, 2209 (1978).

[18] T. Ogawa, J. Phys. Soc. Jpn. Suppl. **52**, 167 (1983).

[19] J. V. José, L. P. Kadanoff, S. Kirkpatrick, and D. R. Nelson, Phys. Rev. B **16**, 1217 (1977).

[20] S. Alexander, Phys. Lett. **54A**, 353 (1975).

[21] R. K. P. Zia and D. J. Wallace, J. Phys. A **8**, 1495 (1975).

[22] J. P. Straley and M. E. Fisher, J. Phys. A **6**, 1310 (1973).

[23] G. R. Golner, Phys. Rev. B **8**, 3419 (1973).

[24] B. Nienhuis, A. N. Berker, E. K. Riedel, and M. Schick, Phys. Rev. Lett. **43**, 737 (1979).